Post-migration image optimization: a Gulf of Mexico case study

Sergey Frolov, Samuel Brown, Sriram Arasanipalai, Nizar Chemingui, Petroleum Geo-Services*

Summary

There are many factors which affect the quality of a subsurface image: acquisition geometry, data quality, accuracy of the subsurface model, imaging algorithm, image post-processing steps, etc. Despite improvements in seismic acquisition, such as full azimuth (FAZ) surveys, and advanced imaging algorithms such as reverse time migration (RTM), focusing energy beneath a complex salt overburden remains a challenging problem. We propose a post-imaging workflow to mitigate migration artefacts, limited illumination problems, and velocity model inaccuracies that cause image distortion. RTM images derived with an inverse scattering imaging condition are decomposed into angle/azimuth domain gathers. The angles and azimuths which constructively interfere at each image point to produce the best image are chosen so as to remove both coherent and incoherent noise and produce an optimal stack. Finally, structure-conformable filtering is applied. We apply this workflow to an RTM image from Garden Banks in the Gulf of Mexico.

Introduction

Complex salt bodies pose a challenging problem for subsalt imaging by any method. Although RTM has become the standard imaging method in Pre-Stack Depth Imaging workflows, challenges arise from the complexity of the medium. These include illumination problems, artefacts coming from back scattering, spurious reflections from multiples and converted waves, and mis-positioned primary reflections due to inaccuracies in the earth model. Illumination problems may be mitigated with Wave-Equation Reflectivity Inversion (Klochikhina et al, 2016; Valenciano et al, 2005). Back scattering noise is accounted for with the use of inverse scattering imaging condition (Whitmore and Crawley, 2012). Imperfections of the model, especially salt geometry, can cause significant distortions of the subsalt image. Decomposing an image into common image gathers (CIGs) takes advantage of imaging redundancy and can aid in evaluating the fidelity of the model used for imaging. In addition, the same decomposition can be used to enhance the quality of the image. Many domains have been proposed over the years, including scalar/vector offsets, incidence/dip angle and azimuth, and shot record decomposition (Xu et al, 2011; Xu et al, 2011). Each one has its' advantages and disadvantages. We choose the incidence angle and azimuth domain for our case study. It naturally provides separation of energy in the case of full azimuth (FAZ) acquisition and the resulting CIGs can be used to tomographically update the velocity model.

Full azimuth acquisition can help illuminate subsalt reflectors in areas with complex salt overburdens. However, due to the challenges mentioned, not all of the energy necessarily focuses in the same place, and coherent and incoherent noise will be present in the CIGs. This provides the motivation for selective stacking. When combining the energy from the CIGs, only the azimuths and angles which contain energy that constructively interfere to produce the best structural image should be included. We present a robust workflow that provides significant uplift to the subsalt image.

RTM azimuth-angle decomposition

During the imaging process of a shot-based RTM, one can estimate incidence angle and azimuth of imaged reflector from source and receiver wavefield direction vectors. The following equation provides a way of estimating an opening angle θ given source and receiver direction vectors ($\mathbf{p}_S$ and $\mathbf{p}_R$, respectively), which can be computed at each time step directly from the wavefields during the propagation process (Whitmore and Crawley, 2012):

$$\theta(\mathbf{p}_S, \mathbf{p}_R) \cong \frac{1}{2}\cos^{-1}\left(\frac{\mathbf{p}_S \cdot \mathbf{p}_R}{|\mathbf{p}_S| \cdot |\mathbf{p}_R|}\right) \quad (1)$$

Angular decomposition of the RTM image benefits from removal of the backscattered energy at each time step. This cannot be done with the cross-correlation imaging condition as the backscattered noise interferes with the data. This low frequency noise can be attenuated using the inverse scattering imaging condition (Whitmore and Crawley, 2012; Stolk et al, 2009). For a fixed moment of time *t*, resulting image at point *x* is given by the following expression:

$$I(x,t) = W_1(x,t)\nabla\Psi_S(x,t) \bullet \nabla\Psi_R(x,T-t) + W_2(x,t)\frac{1}{v^2(x)}\frac{\partial\Psi_S(x,t)}{\partial t}\cdot\frac{\partial\Psi_R(x,T-t)}{\partial t} \quad (2)$$

Here ψ_S and ψ_R are the source and receiver wavefields P_S and P_R, modulated appropriately with ω:

$$\psi_S(x,\omega) = \omega^{-(\alpha+1)/2}\cdot P_S(x,\omega)$$
$$\psi_R(x,\omega) = \omega^{-(\alpha+1)/2}\cdot P_R(x,\omega) \quad (3)$$

Post-migration image optimization: a Gulf of Mexico case study

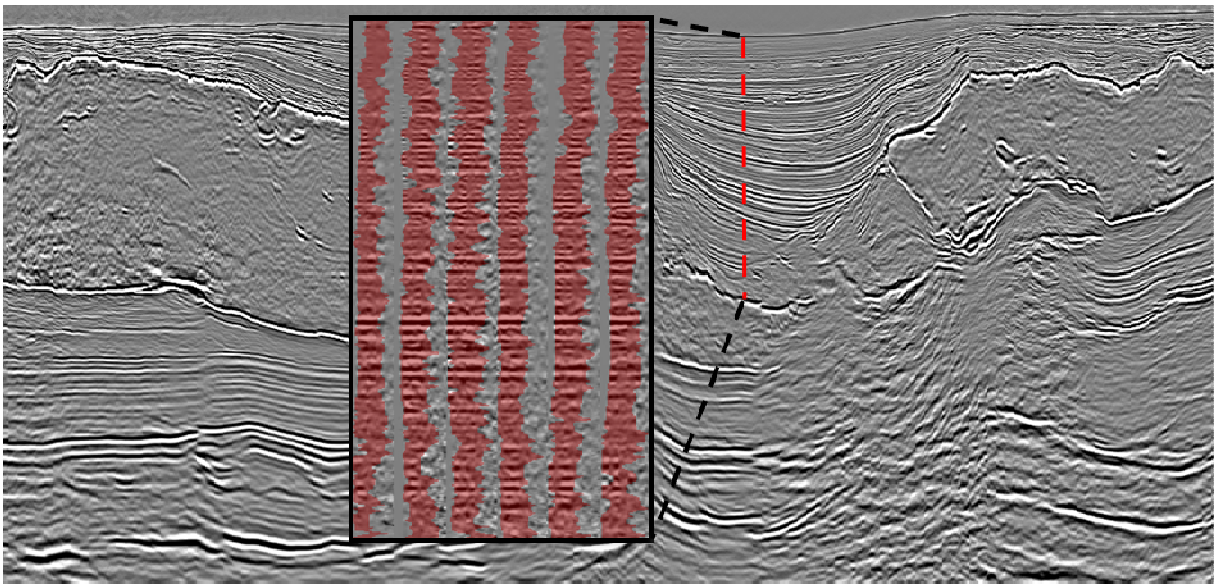

Figure 1: QC of selective stacking: parts of the image kept for stacking (in red) and remaining energy (not highlighted).

The method uses two imaging kernels, a dot product of the gradients of source and receiver wavefields and a product of the time derivatives of the two. When combined with appropriate weights $W_1(x,t)$ and $W_2(x,t)$, these kernels attenuate most of the scattered noise.

A backscatter-free RTM image can then be decomposed into volumes corresponding to different subsurface angles using equation (1). In addition, each volume can be further binned into multiple azimuths. Such decomposition produces a set of azimuth sectored angle gathers $I(x_S, x, \theta, \alpha, t)$, where θ and α indicate incidence angle and azimuth, x_S is the source index, and x is the spatial coordinate. Decomposition of the image into angles and azimuths happens at every image point. This enables post-migration processing and analysis of residual curvature with tomographic model updates.

Image enhancement workflow

There are many methods to improve the image after the migration, ranging from the simple solutions, such as applying mutes or frequency domain filtering to more complicated methods such as structure-conformable smoothing (Clapp, 2001; Hale, 2011). Whereas the simpler methods often don't have any data dependency, i.e. a stationary filter is applied, more complicated methods tend to be data-driven. In the case of structure-oriented filters, the filter orientation and size depends on the data.

Regardless of the way in which slope information is derived to design a filter, whether via structural tensor analysis (Hale, 2011), plane wave destructors (Fomel, 2002) or simple slant-stacking, the result is affected by the quality of the image. In the presence of strong coherent noise, extracting accurate dip information becomes problematic. Before proceeding to this step, it is beneficial to remove spurious reflectors, migration artefacts and other types of noise by performing selective stacking.

The method is based on the following assumption: reliable reflections should be imaged in a similar way in the majority of angle/azimuth volumes. If this is not the case, there is a risk of having a spurious reflection in the image. Vyas (2012) proposed the analysis of a similarity matrix, which is calculated and examined to extract self-similar sets of samples. The sets are ranked based on some criteria and result of the optimized stacking is a collection of images.

Unlike similarity, we choose to analyze the normalized cross-covariance of the contributing images with zero mean $\bar{I}_{iklm}(x)$ and $\bar{I}_{jklm}(x)$:

$$C_{ij}(x) = \frac{\sum_k \sum_l \sum_m \bar{I}_{iklm}(x) \cdot \bar{I}_{jklm}(x)}{\sqrt{\sum_k \sum_l \sum_m \bar{I}_{iklm}(x) \cdot \sum_k \sum_l \sum_m \bar{I}_{jklm}(x)}} \quad (4)$$

here x is a spatial location, i and j are the two volume indices out of the angle-azimuth decomposition, k, l and m are indices over the inlines, xlines and z, respectively.

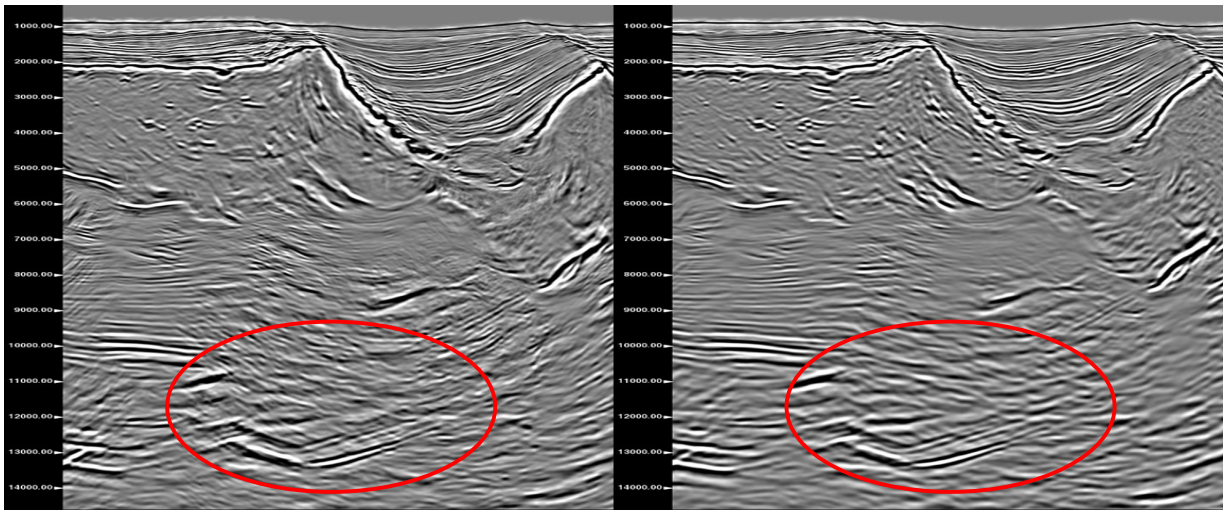

Figure 2: A crossline from the image before (left) and after (right) selective stacking.

We perform a residual moveout correction to align all the contributing images before the analysis, but there is still a chance of a real reflector not being imaged in the same place in all the volumes. In the extreme case of opposite polarity, cross-covariance will be able to capture that.

Zero-lag analysis doesn't show the complete picture, so we calculate a lagged cross-covariance matrix. We perform the analysis in spatially overlapping windows. For a chosen method of decomposition (incidence angle and azimuth), for a given window, there is a 5D search space to analyze $C_{ij}(\tau)$ (two dimensions from mutual correlation of volumes *i* and *j*, and three more from spatial lags $\tau = (\tau_x \tau_y \tau_z)$). To reduce the dimensionality of the problem, one can come up with a weighted metric based on information from the lagged covariances:

$$C_{ij}(x) = \sum_{\tau} w(\tau) \cdot C_{ij}(\tau) \quad (5)$$

After the matrix is formed, we tried analyzing clusters of similar traces as proposed by Vyas. Rather than dealing with the collections of mutually similar volumes, we decided to find parts of the image that have the least similarity with the rest and iteratively exclude those from stacking. This approach minimizes the chances that coherent parts of the image will be lost. Essentially the algorithm performs a local 5D analysis to extract the pieces of data that look alike.

Figure 1 shows a segment of a QC volume produced after selective stacking. Parts of the image that were kept for stacking are in red, removed data is not highlighted. The algorithm is able to delineate the extent of the signal. Figure 2 shows that after selective stacking the image has a higher signal-to-noise ratio, and the reflectors appear more continuous and coherent. The de-noising effect is more noticeable in the zones in which coherent noise with conflicting dip interferes with well-focused reflectors.

In cases where the selection was not too aggressive, and there are volumes with coherent noise left for stacking, we can further separate similar volumes from the rest by providing adjusted weights:

$$I(x) = \sum_{i} w_i(x) \cdot \overline{I_i}(x) \quad (6)$$

Nadaraya and Watson (1964) proposed a method for non-parametric regression. The result of kernel application is given by the following equation:

$$I(x) = \sum_{i} w_i(x) \cdot I_i(x) / \sum_{j} w_j(x) \quad (7)$$

Weights w_i are based on a kernel K of certain width h:

$$w_i(x) = \sum_{j} K_h(I_j - I_i) \quad (8)$$

For our case study, we used Gaussian kernel. There is a free parameter *h* that controls how neighborhoods of similar data will be weighted. Li and Zhou (2015) discuss methods to obtain optimal parameterizations for the kernel. After the image is cleaned up, we can safely apply structure-conformable smoothing to further improve the image.

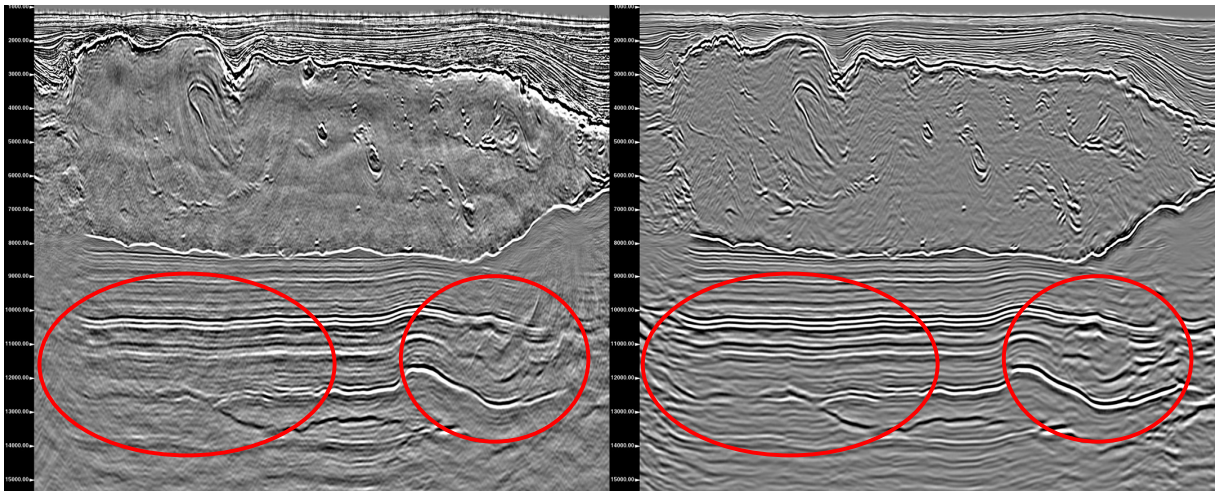

Figure 3: An inline from the survey before (left) and after (right) image enhancement workflow.

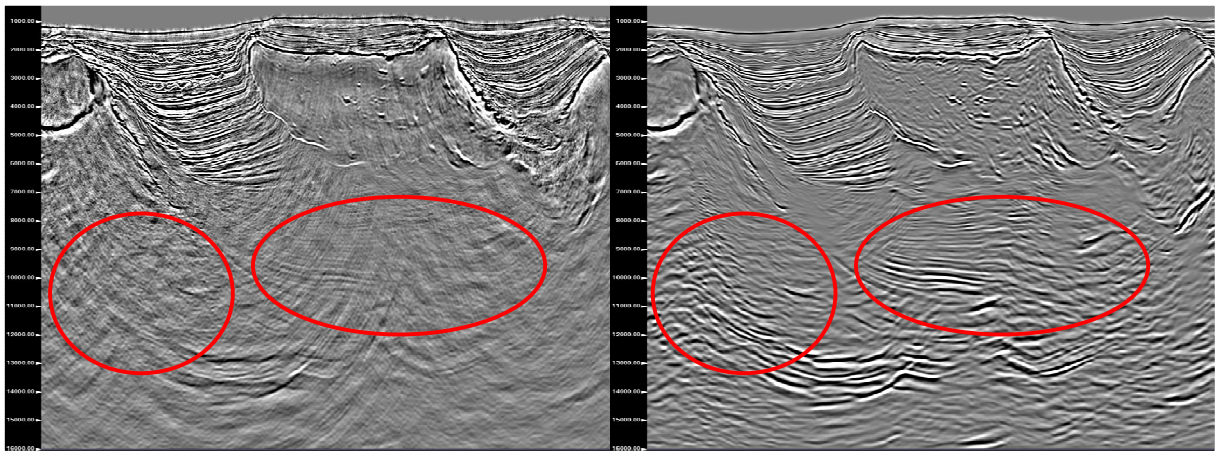

Figure 4: A crossline from the survey before (left) and after (right) image enhancement workflow.

Data Example

We have applied the workflow to a large FAZ survey from the Gulf of Mexico. Subsalt areas of Garden Banks are especially difficult to image, mostly due to complexity of the top salt. The survey has been acquired along 3 azimuths with maximum offsets of 16 km, providing more energy to image deep subsalt structures. As a result of image enhancement workflow, the stacks in Figures 3 and 4 are greatly improved. Subsalt reflectivity is enhanced, while coherent and incoherent noise has been attenuated.

Conclusions

Complex salt geometries pose many challenges to modern imaging algorithms. The quality of the image can be significantly improved by applying post-migration image processing. Angle and azimuth decomposition of the image provides natural energy separation for FAZ acquisition. Selective stacking provides separation of coherent signal and various types of noises. Better image quality leads to better estimates of reflector dips, which in turn allows more stable application of structure-conformable filtering. Our workflow was demonstrated on a FAZ dataset from a challenging area of the Gulf of Mexico.

Acknowledgements

We would like to thank PGS for permission to present this paper. We acknowledge the PGS processing team for providing intermediate processing results.

EDITED REFERENCES

Note: This reference list is a copyedited version of the reference list submitted by the author. Reference lists for the 2016 SEG Technical Program Expanded Abstracts have been copyedited so that references provided with the online metadata for each paper will achieve a high degree of linking to cited sources that appear on the Web.

REFERENCES

Clapp, R. G., 2001, Geologically constrained migration velocity analysis: Ph.D. thesis, Stanford University.

Fomel, S., 2002, Applications of plane-wave destruction filters: Geophysics, **67**, 1946–1960, http://dx.doi.org/10.1190/1.1527095.

Hale, D., 2011, Structure-oriented bilateral filtering of seismic images: 81st Annual International Meeting, SEG, Expanded Abstracts, 3596–3600, http://dx.doi.org/10.1190/1.3627947.

Klochikhina, E., S. Lu, A. A. Valenciano, and N. Chemingui, 2016, Subsalt imaging by wave equation reflectivity inversion: 78th Annual International Conference and Exhibition, EAGE, Extended Abstracts.

Li, F., and Y. Zhou, 2015, Parameter estimation for Nadaraya-Watson kernel regression method with small samples: Recent Researches in Applied Mathematics, Simulation and Modelling, 22–29.

Nadaraya, E. A., 1964, On estimating regression: Theory of Probability and its Applications, **9**, 141–142, http://dx.doi.org/10.1137/1109020.

Stolk, C., M. V. de Hoop, and T. Op't Root, 2009, Reverse time migration-inversion from single-shot data: 79th Annual International Meeting, SEG, Expanded Abstracts, 2995–2999.

Valenciano, A. A., B. Biondi, and A. Guitton, 2005, Target-oriented wave-equation inversion: 70th Annual International Meeting, SEG, Expanded Abstracts, 1662–1665, http://dx.doi.org/10.1190/1.2148015.

Vyas, M., and A. Sharma, 2012, Optimal stacking: 83rd Annual International Meeting, SEG, Expanded Abstracts, 1–5, http://dx.doi.org/10.1190/segam2012-1240.1.

Whitmore, N. D., and S. Crawley, 2012, Applications of RTM inverse scattering imaging conditions: 83rd Annual International Meeting, SEG, Expanded Abstracts, 1–6, http://dx.doi.org/10.1190/segam2012-0779.1.

Xu, Q., Y. Li, X. Yu, and Y. Huang, 2011, Reverse time migration using vector offset output to improve subsalt imaging — A case study at the walker ridge GOM: 81st Annual International Meeting, SEG, Expanded Abstracts, 3268–3274, http://dx.doi.org/10.1190/1.3627875.

Xu, S., Y. Zhang, and B. Tang, 2011, 3D angle gathers from reverse time migration: Geophysics, **76**, no. 2, S77–S92, http://dx.doi.org/10.1190/1.3536527.